



## UvA-DARE (Digital Academic Repository)

### Subtalar joint kinematics and arthroscopy: insight in the subtalar joint range of motion and aspects of subtalar joint arthroscopy

Beimers, L.

**Publication date**  
2012

[Link to publication](#)

#### **Citation for published version (APA):**

Beimers, L. (2012). *Subtalar joint kinematics and arthroscopy: insight in the subtalar joint range of motion and aspects of subtalar joint arthroscopy*. [Thesis, fully internal, Universiteit van Amsterdam].

#### **General rights**

It is not permitted to download or to forward/distribute the text or part of it without the consent of the author(s) and/or copyright holder(s), other than for strictly personal, individual use, unless the work is under an open content license (like Creative Commons).

#### **Disclaimer/Complaints regulations**

If you believe that digital publication of certain material infringes any of your rights or (privacy) interests, please let the Library know, stating your reasons. In case of a legitimate complaint, the Library will make the material inaccessible and/or remove it from the website. Please Ask the Library: <https://uba.uva.nl/en/contact>, or a letter to: Library of the University of Amsterdam, Secretariat, P.O. Box 19185, 1000 GD Amsterdam, The Netherlands. You will be contacted as soon as possible.

CHAPTER 3

**In-vivo range of motion of the subtalar joint using  
computed tomography**

L. Beimers, G.J.M. Tuijthof, L. Blankevoort, R. Jonges, M. Maas, C.N. van Dijk

*Journal of Biomechanics* 2008;41(7):1390-1397

## ABSTRACT

**Background** Understanding in-vivo subtalar joint kinematics is important for evaluation of subtalar joint instability, the design of a subtalar prosthesis and for analysing surgical procedures of the ankle and hindfoot. No accurate data are available on the normal range of subtalar joint motion. The purpose of this study was to introduce a method that enables the quantification of the extremes of the range of motion of the subtalar joint in a loaded state using multidetector computed tomography (CT) imaging.

**Methods** In 20 subjects, an external load was applied to a footplate and forced the otherwise unconstrained foot in eight extreme positions. These extreme positions were foot dorsiflexion, plantarflexion, eversion, inversion and four extreme positions in between the before mentioned positions. CT images were acquired in a neutral foot position and each extreme position separately. After bone segmentation and contour matching of the CT data sets, the helical axes were determined for the motion of the calcaneus relative to the talus between four pairs of opposite extreme foot positions. The helical axis was represented in a coordinate system based on the geometric principal axes of the subjects' talus.

**Results** The greatest relative motion between the calcaneus and the talus was calculated for foot motion from extreme eversion to extreme inversion (mean rotation about the helical axis of  $37.3 \pm 5.9^\circ$ , mean translation of  $2.3 \pm 1.1$  mm).

**Conclusion** A consistent pattern of range of subtalar joint motion was found for motion of the foot with a considerable eversion and inversion component.

## INTRODUCTION

The subtalar joint has an important role in the complex hindfoot motion during gait.<sup>4,8,14</sup> Subtalar joint instability has received increasing attention in the literature as a cause of hindfoot instability. No consensus exists regarding the diagnostic criteria for subtalar joint instability.<sup>3,24</sup> One of the underlying causes is the lack of a standard method for accurately measuring subtalar joint motion. In addition, there are no clear reference values of normal subtalar joint motion. For the evaluation of subtalar joint instability accurate knowledge of the reference values of subtalar joint motion is necessary. Currently, for end-stage osteoarthritis of the subtalar joint unresponsive to conservative treatment the only operative option is a subtalar arthrodesis. Fournol reported a series of 100 implanted prostheses to replace subtalar arthrodesis for post-traumatic osteoarthritis.<sup>7</sup> Over 50% of the patients had unsatisfactory results, mostly because of failure of the prosthesis. Better outcomes are expected with an improved design of the subtalar prosthesis. For this development, kinematic data of the subtalar joint are essential. In addition, an accurate quantitative data set of subtalar joint motion is required for the validation of biomechanical computer models of the ankle joint complex and for studying the kinematic effects of ankle and hindfoot surgery.

The lack of external landmarks of the talus in combination with the subtalar joint geometry has made the subtalar joint kinematics difficult to investigate in living subjects. In-vivo studies on subtalar kinematics used camera registration techniques of external surface markers attached to the skin during stance and walking. It is obvious that this technique cannot accurately measure rotations and translations of the bones of the subtalar joint.<sup>5,12,13,19,25</sup> The invasive roentgen stereophotogrammetric analysis (RSA) has been considered an accurate technique for studying bone-to-bone motion in-vivo and was used by numerous authors to study ankle and foot kinematics.<sup>2,16,27</sup> It is however a cumbersome method and also has the risk of infection and damaging the joint cartilage due to malpositioning of the bone markers. More recently, computed tomography (CT) and magnetic resonance imaging (MRI) techniques were used to study the ankle and subtalar joint motion in cadaveric specimens and living subjects.<sup>18,21-23,26</sup> None of these studies reported on the extremes of the range of motion of the subtalar joint in-vivo. The purpose of this study was to introduce an accurate method that enables the quantification of the extremes of bone-to-bone motion in a loaded state using multidetector CT imaging. The method was applied to acquire a reference data set of the normal extremes of subtalar joint motion in a group of volunteers.

## METHODS

The study was approved by the Medical Ethical Committee of our hospital. Twenty healthy volunteers (10 males, 10 females) signed informed consent prior to participation. The mean age in this group was 26.3 years, ranging from 22 to 35 years. None of the volunteers had any ankle/foot complaints, nor had a history of ankle/foot trauma or underwent surgery of the lower extremities. Physical examination of the ankle and hindfoot was performed to check for any abnormalities. Each subject was positioned on the scanner table in a supine position with the right lower leg fixed to the supporting platform using velcro straps (Fig. 1). The supporting platform was positioned 10 cm above the scanner table allowing for slight flexion of the knee, thereby relaxing the ankle/foot. The right foot sole was placed on a customized footplate that was made from radiolucent materials. The foot was fixed to the footplate with two velcro straps around the ankle and the forefoot. The footplate was fabricated by the Medical Technical Development Department of our hospital.

For computer segmentation of the talus and calcaneus, the first series of CT images of the right ankle and hindfoot was acquired with the foot in a neutral position relative to the lower leg (i.e. the sole of the foot was placed in approximately 90° relative to the anterior rim of the tibia). This neutral position with no stress applied to the subtalar joint was necessary as computer segmentation of one particular bone is more difficult with the articular surfaces of the joint having contact. Bone segmentation is the process of making a three-dimensional computer representation of a particular bone based on the automatic detection of the outer osseous surface of the bone in a CT data set using a radiation dose of 150 mAs/slice. This step is necessary to be able to determine the exact location of the same bone in a different CT data set with a low radiation dose scanning technique. In this study the Philips MX8000 multidetector CT scanner was used (Philips Medical Systems, The Netherlands). The scanner settings are shown in Table 1. An external load (i.e. weighted sandbags) was applied to the footplate through a system of a wire and pulleys to force the foot in eight extreme positions. The footplate had eight fixed attachment points for the pulling wire located at the periphery of the footplate. In all instances, the pulling force of the external load to the footplate through the wire was directed cranially. The eight extreme foot positions resulting from the load applied to the footplate were the following: dorsiflexion, combined eversion-dorsiflexion, eversion, combined eversion-plantarflexion, plantarflexion, combined inversion-plantarflexion, inversion, and, combined inversion-dorsiflexion. CT scanning was performed in each of the eight extreme foot positions starting from dorsiflexion (assigned position 1) and continued in

a clockwise order to end with position 8. Approximately 2 cm of the distal tibia, the complete talus, the calcaneus, the navicular and the cuboid bone were scanned. In each extreme foot position, a series of CT images was acquired with a low radiation dose technique (26 mAs/slice). The total external load that was applied in each of the extreme foot positions was the maximum load that was tolerated by the subject. The means of the external loads applied to the footplate to force the foot in the eight extreme positions ranged from 58 to 62 N. The relaxed status of the lower leg muscles was checked by asking the subjects and by palpation of the muscles.

A workstation (IBM RS 6000) was used for image processing and visualization. Software was developed in C and C++ to implement segmentation and registration algorithms. For reconstruction of the CT images data an image matrix of 512×512 pixels was used. The pixel size of 0.3 mm and the slice interval of 0.3 mm resulted in a volume of isotropic voxels (voxel size 0.3×0.3×0.3 mm<sup>3</sup>). First, bone segmentation of the talus and calcaneus was performed by a region growing algorithm using the regular dose CT scan images with the right foot in a neutral position. With this technique for each voxel a weighted grey value mean was calculated using a small sphere (radius of 0.5 mm). Whenever the spherical grey value mean was higher than a predefined grey value this voxel was classified as bone tissue and assigned to the bone region in the process of growing. The region growing algorithm was able to automatically find the outline of the bone structure in most cases but did not always comprise the inner bone structure. To close the boundaries of the bones and completing the registration of the inner and outer bone structure, an additional procedure based on binary operators was used. In the second step, the talus and calcaneus were matched in the low-dose CT data sets with the foot in the eight extreme positions. The boundary voxels of each bone in the regular dose CT scans were matched with the corresponding boundary voxels of the bones in the low-dose CT scans. To speed up computation, a randomly chosen subset of the boundary voxels of each bone was used for the first stage in the matching procedure. A cost function based on grey value correlation of the boundary voxels of each bone was minimized. The downhill simplex method by Nelder and Mead was used to minimize the cost function between the grey values of the regular dose and the low-dose scan.<sup>20</sup> The matching procedure required a rough estimate of the rotation and translation parameters of the bones. This was done by visually overlying the centers of gravity of the corresponding bones in the low-dose CT data sets. Next, the matching software was able to find an optimal fit in a three-dimensional search window around each bone. In the second step both translation and rotation parameters for

each bone were optimized starting from the optimal position in the search window. In this final step, all boundary voxels of the bones were used to gain an accurate estimation of all rotation and translation parameters. In all instances, the centre of gravity of the segmented bone structure was defined as the origin of the embedded coordinate system.

For quantitative analysis of subtalar joint kinematics, the helical axis parameters for motion of the calcaneus relative to the talus between opposite extreme foot positions were computed. The helical transformation is expressed in terms of a rotation about a helical axis, and a translation along this axis.<sup>28,29</sup> The helical axis was represented in a right-hand rule XYZ-coordinate system based on the geometric principal axes of the talus of the subject (Fig. 2). The origin of the talus-based coordinate system was placed in the centroid of the talus. To define the orientation of the helical axis in the XYZ-coordinate system, the inclination and deviation angle of the helical axis was calculated for each testing subject. The inclination angle is defined as the angle between the helical axis and the XY-plane. The deviation angle is defined as the angle between the projection of the helical axis on the XZ-plane and the X-axis. A positive value of the deviation angle of the helical axis indicates a medially orientated helical axis in an anterior direction. In addition, the absolute angle between the helical axis of one subject and the mean helical axis of the 20 subjects was calculated. The helical axis parameters were calculated with mathematical routines developed in Matlab software (Matlab Version 6.5, The MathWorks Inc., Natick, United States of America) using a Pentium 4 processor type computer (Hewlett-Packard, United States of America) running Microsoft Operating System Windows XP Professional (Microsoft Corporation, United States of America).

## RESULTS

The position of the calcaneus relative to the fixed talus in the eight extreme foot positions for one subject is shown in Fig. 3(A, B). Two consistent extreme positions of the calcaneus relative to the talus were observed, i.e. extreme eversion and extreme inversion, irrespective of the combination with plantarflexion or dorsiflexion of the foot. The helical axes that represented the range of motion of the subtalar joint between two opposite extreme foot positions, were consistent in the group of 20 subjects, except for the motion between dorsiflexion and plantarflexion (Fig. 4; Table 2, Table 3, Table 4 and Table 5). The inclination angle of the helical axes of the motion between extreme eversion and inversion, with and without combined dorsiflexion and plantarflexion, showed a good consistency with a standard

deviation ranging from 4.0° to 4.8° (Table 2, Table 3 and Table 4). Comparable results were found for the absolute angles between the helical axes of the subjects and the mean helical axis for foot motion with a considerable eversion and inversion component (Table 2, Table 3, Table 4 and Table 5).

The range of motion of the subtalar joint as expressed by the rotation about the helical axis was on average the highest for the motion between extreme eversion and extreme inversion (37.3±5.9°) (Table 2, Table 3 and Table 4). The translation values for this type of subtalar joint motion were ranging from 0.2 to 5.1 mm. No correlation between the external loads applied to the footplate and the range of subtalar joint motion was found. In addition, there was no significant difference in outcome between male and female range of subtalar joint motion. The subtalar joint motion for extreme dorsiflexion to extreme plantarflexion of the foot was highly variable among the subjects as is shown by a large variation of the direction of the helical axes. Rotation, translation values and absolute helical axis angles were also highly variable for this type of subtalar joint motion (Fig. 4D; Table 5).

To assess the reproducibility of the CT scanning technique, in one subject a repeated scan was acquired with the foot in the extreme eversion position (position 3) after completing the protocol. The subject was not removed from the device for the repeated scan. The orientation of the helical axes for motion between the neutral position to extreme eversion appeared to be reproducible. For the repeated scan the rotation difference was 1.0° (23.8° versus 24.8° for the initial scan) and the translation differed 0.2 mm (1.5 mm versus 1.7 mm for the initial scan).

## DISCUSSION

The extremes of the range of motion of the calcaneus relative to the talus in a loaded state in healthy subjects using a multidetector CT scanner were studied. For extreme positions of the foot with a considerable eversion and inversion component, the helical axis parameters for the subtalar joint were consistent between the subjects in our series. We found the helical axis of the right-sided subtalar joint running from postero-lateral-inferior to antero-medial-superior. This finding is in agreement with the literature.<sup>1,6,9-11,15,17</sup> In contrast to other studies, we found a relatively little variation in the inclination angle, and moderate variation in the deviation angle of the mean helical axis for extreme foot positions with an eversion and inversion component.<sup>11,27</sup> This might result from the talus-based coordinate system that was defined for every testing subject individually. The subtalar joint motion from extreme dorsiflexion to extreme plantarflexion of the foot resulted in widely varying helical axis

parameters in our series and it was apparent that the subtalar joint was not in stable end positions.

Our study was the first to measure subtalar joint motion between the opposite extreme foot positions in a loaded state in-vivo using CT images. The greatest relative motion between the calcaneus and the talus was found for extreme eversion to extreme inversion of the foot and the mean subtalar joint rotation about the helical axis measured  $37.3 \pm 5.9^\circ$  (range  $26.6$ – $50.4^\circ$ ). CT and MRI techniques have been used for quantifying ankle joint motion between predefined input foot positions in-vivo.<sup>18,22,26</sup> Others studied the response of the ankle and subtalar joint in-vivo to an inversion load and an anterior drawer load using an MRI technique.<sup>21,23</sup> Outcomes of these studies are difficult to compare with the variation of coordinate systems and joint motion definitions used. The advantage of MRI over CT is that no radiation is used. However, the CT scanning technique is preferred as it is time efficient and the most suitable imaging technique for computer bone segmentation and bone matching. In addition, in this study we used a low-dose technique for CT scanning of the eight extreme foot positions. Fewer scans may be required clinically for assessment of subtalar joint function by studying a limited number of extreme foot positions, thereby reducing the radiation dose. Reproducibility of the technique presented was not fully assessed in this study. Cadaveric specimens proved not useful for reproducibility tests as bone segmentation and matching was more difficult than in living bone due to the inferior quality of the cadaveric bones. Re-testing of human volunteers was not performed, as this was not the subject of the current study. This study presents a technique for quantitative analysis of bone-to-bone motion in a loaded state with the otherwise unconstrained foot in healthy volunteers. With the present study we aimed at providing kinematic data on the subtalar joint that is useful for both clinicians and researchers. It is of value from a basic-science perspective as the subtalar joint function is a subject of increasing interest. Secondly, this study is important from a clinical point of view because many problems that arise in the hindfoot are thought to be associated with an alteration of subtalar joint motion.

#### Acknowledgements

Mr. M. Poulus and Ms. M.A. de Graaf (Department of Radiology, University Hospital AMC, Amsterdam, The Netherlands) are thanked for the assistance with acquiring CT images.

Mr. P. Broekhuijsen and colleagues (The Department for Medical Technical Development (M.T.O.), University Hospital AMC, Amsterdam, The Netherlands) are thanked for development of the footplate for CT scanning.

#### REFERENCES

1. **Alexander RE, Battye CK, Goodwill CJ, Walsh JB.** The ankle and subtalar joints. *Clinical Rheumatic Disease*. 1982;8(3):703–711.
2. **Benink RJ.** The constraint-mechanism of the human tarsus. A roentgenological experimental study. *Acta Orthopaedica Scandinavica Supplementum*. 1985;215:1–135.
3. **Budny A.** Subtalar joint instability: current clinical concepts. *Clinical Podiatric Medical Surgery*. 2004;21(3):449–460.
4. **Close JR, Inman VT, Poor PM, Todd FN.** The function of the subtalar joint. *Clinical Orthopaedic*. 1967;50:159–179.
5. **Cornwall MW, McPoil TG.** Three-dimensional movement of the foot during the stance phase of walking. *Journal of American Podiatric Medical Association*. 1999;89(2):56–66.
6. **Engsberg JR.** A biomechanical analysis of the talocalcaneal joint—in-vitro. *Journal of Biomechanics*. 1987;20(4):429–442.
7. **Fournol S.** L'arthroplastie totale sous-talienne. Resultats et bilan d'une serie de 100 protheses. *Medical Chirurgie Pied*. 1999;15(2):67–71.
8. **Huson A.** Functional anatomy of the foot. In: Jahhs, M.H., (Ed.), Disorders of the Foot and Ankle. Medical and Surgical Management, (Second ed.), WB Saunders (1991), pp. 409–431.
9. **Huson A.** Biomechanics of the tarsal mechanism. A key to the function of the normal human foot. *Journal of American Podiatric Medical Association*. 2000;90(1):12–17.
10. **Inman VT.** The Joints of the Ankle, Williams & Wilkins Company, Baltimore (1976).
11. **Isman RE, Inman VT.** Anthropometric studies of the human foot and ankle. *Bulletin of Prosthetics Research*. 1969;10:97–129.
12. **Kadaba MP, Ramakrishnan HK, Wootten ME.** Measurement of lower extremity kinematics during level walking. *Journal of Orthopaedics Research*. 1990;8(3):383–392.
13. **Kepple TM, Stanhope SJ, Lohmann KN, Roman NL.** A video-based technique for measuring ankle-subtalar motion during stance. *Journal of Biomedical Engineering*. 1990;12(4):273–280.
14. **Lapidus PW.** Subtalar joint, its anatomy and mechanics. *Bulletin of Hospital Joint Diseases*. 1955;16(2):179–195.
15. **Leardini A, Stagni R, O'Connor JJ.** Mobility of the subtalar joint in the intact ankle complex. *Journal of Biomechanics*. 2001;34(6):805–809.
16. **Lundberg A.** Kinematics of the ankle and foot. In-vivo roentgen stereophotogrammetry. *Acta Orthopaedica Scandinavica Supplementum*. 1989;233:1–24.
17. **Manter JT.** Movements of the subtalar and transverse tarsal joints. *The Anatomical Record*. 1941;80(4):397–410.
18. **Metz-Schimmerl SM, Bhatia G, Vannier MW.** Visualization and quantitative analysis of talocrural joint kinematics. *Computer Medical Imaging Graph*. 1994;18(6):443–448.
19. **Moseley L, Smith R, Hunt A, Gant R.** Three-dimensional kinematics of the rearfoot during the stance phase of walking in normal young adult males. *Clinical Biomechanics*. 1996;11(1):39–45.
20. **Nelder JA, Mead R.** A simplex method for function minimization. *The Computer Journal*. 1965;7:308–313.
21. **Ringleb SI.** A three-dimensional stress MRI technique to quantify the mechanical properties of the ankle and subtalar Joint—Application to the diagnosis of ligament injuries, Drexel University (2003).
22. **Sheehan FT, Seisler AR, Siegel KL.** In-vivo talocrural and subtalar kinematics: a non-invasive 3D dynamic MRI study. *Foot Ankle International*. 2007;28(3):323–335.
23. **Siegler S, Udupa JK, Ringleb SI, Imhauser CW, Hirsch BE, Odhner D, Saha PK, Okereke E, Roach N.** Mechanics of the ankle and subtalar joints revealed through a 3D quasi-static stress MRI technique. *Journal of Biomechanics*. 2005;38(3):567–578.

24. **Sijbrandij ES, van Gils AP, van Hellemond FJ, Louwerens JW, de Lange EE.** Assessing the subtalar joint: the Brodén view revisited. *Foot Ankle International*. 2001;22(4):329–334.
25. **Tranberg R, Karlsson D.** The relative skin movement of the foot: a 2-D roentgen photogrammetry study. 1. *Clinical Biomechanics*. 1998;13(1):71–76.
26. **Udupa JK, Hirsch BE, Hillstrom HJ, Bauer GR, Kneeland JB.** Analysis of in-vivo 3-D internal kinematics of the joints of the foot. *IEEE Transactions on Biomed Eng*. 1998;45(11):1387–96.
27. **van Langelaan EJ.** A kinematical analysis of the tarsal joints. An X-ray photogrammetric study. *Acta Orthopædica Scandinavica Supplementum*. 1983;204:1–269.
28. **Woltring HJ, Huiskes R, de Lange A, Veldpaus FE.** Finite centroid and helical axis estimation from noisy landmark measurements in the study of human joint kinematics. *Journal of Biomechanics*. 1985;18(5):379–389.
29. **Woltring HJ, Long K, Osterbauer PJ, Fuhr AW.** Instantaneous helical axis estimation from 3-D video data in neck kinematics for whiplash diagnostics. *Journal of Biomechanics*. 1994;27(12):1415–1432.

## TABLES

**Table 1** Settings of the Philips MX8000 multidetector CT scanner (Philips Medical Systems, The Netherlands) for scanning of the ankle and hindfoot in the neutral position and the eight extreme positions

Parameter	Neutral position	Extreme positions
Gantry tilt (deg)	0	0
Field of view (mm)	154	154
Slice thickness (mm)	0.6	0.6
Increment (mm)	0.3	0.3
Image matrix (Row×Column, Isotope volume)	512×512	512×512
Pitch	0.875	0.875
Rotation time (s)	0.75	0.75
Resolution	Ultra high	Ultra high
Radiation dose	150 mAs/slice	26 mAs/slice
Reconstruction filter setting	C	C

**Table 2** Helical axis parameters for the subtalar motion from extreme eversion to extreme inversion

Subject no.	Inclination angle (deg)	Deviation angle (deg)	Rotation (deg)	Translation (mm)	Absolute angle (deg)
1	48.2	3.8	37.7	1.7	3.6
2	54.2	14.1	32.0	1.4	5.8
3	52.5	12.1	35.4	0.4	4.3
4	45.7	-3.1	46.1	4.1	8.1
5	47.8	22.7	31.2	0.6	11.9
6	59.1	-1.3	41.6	2.8	8.3
7	50.1	1.2	36.4	2.9	3.0
8	58.7	7.6	36.5	2.5	7.2
9	53.8	3.9	34.7	2.5	2.3
10	46.2	-0.9	33.9	4.3	6.8
11	54.9	5.0	44.7	2.9	3.2
12	48.9	10.7	29.0	1.5	4.4
13	45.4	4.2	39.0	3.1	6.3
14	48.8	-9.4	26.6	1.8	9.8
15	56.5	7.0	38.4	1.0	4.9
16	45.2	-4.9	41.2	1.9	9.3
17	51.2	16.7	50.4	4.0	7.1
18	53.5	3.6	41.9	2.3	2.1
19	52.5	12.2	32.5	2.6	4.3
20	55.3	3.2	37.6	1.9	3.8
<b>Mean</b>	51.4	5.4	37.3	2.3	5.8
<b>S.D.</b>	4.3	7.8	5.9	1.1	6.4

**Table 3** Helical axis parameters for the subtalar motion from extreme combined eversion-dorsiflexion to extreme combined inversion-plantarflexion

Subject no.	Inclination angle (deg)	Deviation angle (deg)	Rotation (deg)	Translation (mm)	Absolute angle (deg)
1	46.8	5.3	34.2	1.8	6.1
2	52.1	22.9	22.5	0.3	7.0
3	50.0	19.4	24.7	0.6	5.0
4	48.9	6.5	35.0	1.2	4.0
5	45.5	23.1	27.2	0.7	9.4
6	59.5	5.4	31.3	1.5	9.1
7	48.8	8.9	30.8	1.8	3.0
8	56.9	14.4	30.6	2.0	6.0
9	53.9	8.9	29.3	1.5	3.3
10	48.3	10.0	24.9	2.1	3.0
11	57.0	21.1	32.6	-0.2	8.0
12	48.7	13.0	26.0	1.2	2.6
13	46.8	8.2	28.9	1.7	4.9
14	50.8	-4.3	22.5	1.3	10.1
15	55.4	9.2	32.6	0.4	4.5
16	46.4	-3.7	38.2	1.7	11.2
17	47.6	20.4	41.5	1.4	6.7
18	48.0	12.1	29.7	0.8	3.2
19	52.5	20.5	24.9	1.0	5.6
20	53.7	14.4	25.8	0.3	3.1
<b>Mean</b>	50.9	11.8	29.7	1.2	5.8
<b>S.D.</b>	4.0	8.0	5.1	0.7	6.3

**Table 4** Helical axis parameters for the subtalar motion from extreme combined eversion-plantarflexion to extreme combined inversion-dorsiflexion

Subject no.	Inclination angle (deg)	Deviation angle (deg)	Rotation (deg)	Translation (mm)	Absolute angle (deg)
1	48.6	1.9	38.9	1.7	2.7
2	51.2	12.2	31.9	2.7	6.1
3	53.4	12.6	30.9	2.1	6.6
4	40.1	-12.7	37.3	4.4	15.3
5	46.6	21.6	26.8	1.1	13.4
6	58.9	-3.1	41.6	3.1	8.3
7	51.7	-3.3	32.6	3.0	3.6
8	57.2	-3.8	34.6	3.0	7.0
9	53.8	-2.0	30.5	2.4	3.7
10	44.7	-6.0	32.9	5.1	8.6
11	53.7	-3.3	46.0	4.2	4.3
12	49.9	9.7	28.2	1.6	4.8
13	44.5	4.1	36.6	3.8	6.8
14	49.5	-7.1	29.8	3.0	6.3
15	53.5	6.5	34.5	1.9	3.4
16	45.0	-6.7	39.3	2.6	8.7
17	52.2	16.3	48.0	4.8	8.6
18	53.3	2.8	41.4	2.5	2.1
19	53.2	10.0	32.1	2.6	5.0
20	57.1	1.4	36.8	1.7	5.9
<b>Mean</b>	50.9	2.5	35.5	2.9	6.6
<b>S.D.</b>	4.8	8.9	5.7	1.1	7.3

**Table 5** Helical axis parameters for the subtalar motion from extreme dorsiflexion to extreme plantarflexion

Subject no.	Inclination angle (deg)	Deviation angle (deg)	Rotation (deg)	Translation (mm)	Absolute angle (deg)
1	-42.9	-6.1	21.0	2.8	4.2
2	-45.4	-2.3	8.2	3.7	5.5
3	-32.0	3.0	5.0	2.4	17.3
4	66.3	58.4	8.6	-0.6	32.4
5	50.8	24.8	7.5	-0.3	10.8
6	-53.0	3.6	24.5	3.5	11.3
7	61.7	19.7	5.6	-1.1	16.6
8	66.6	64.3	4.2	-1.2	34.8
9	59.2	51.7	7.7	-1.0	27.9
10	-21.5	16.7	12.8	4.5	32.8
11	11.0	-6.8	4.1	5.5	57.1
12	69.0	86.8	1.6	-0.2	45.4
13	23.1	50.5	2.8	0.5	88.2
14	-9.7	9.8	3.7	2.8	40.1
15	-2.9	-20.2	2.6	3.4	44.1
16	52.6	42.8	3.6	1.0	71.5
17	-33.3	14.3	6.2	4.3	22.5
18	-44.2	-1.0	5.3	1.7	6.7
19	57.0	64.1	2.4	-0.6	34.3
20	-43.0	-1.9	9.3	3.1	6.6
<b>Range<sup>(a)</sup></b>					
<b>min.</b>	-53.0	-20.2	1.6	-1.2	4.2
<b>max.</b>	69.0	86.8	24.5	5.5	88.2

(a) Means and standard deviations were not calculated as the helical axis values were highly variable for this range of subtalar joint motion.

## FIGURES



**Figure 1** The subject was positioned on the CT table with the right lower leg attached to the supporting platform and with the right foot attached to the footplate. An external load was applied to the footplate to force the otherwise unconstrained foot in the eight extreme positions. Following CT scanning with the foot in the neutral position, scanning was performed for each of the extreme positions separately.

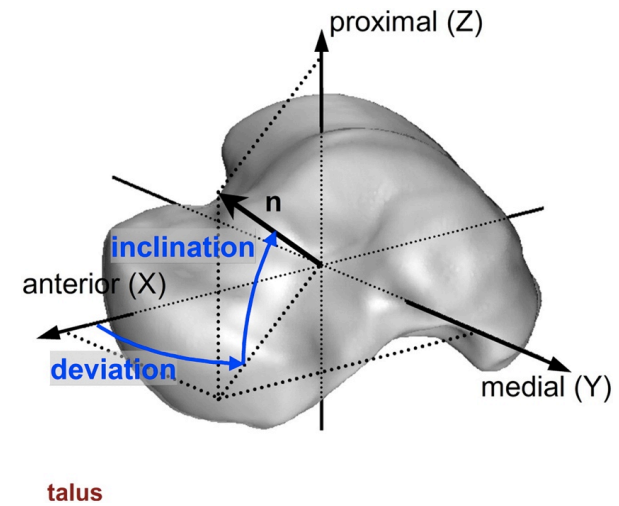


**Figure 2** For each subject, the helical axis for subtalar joint motion was represented in a XYZ-coordinate system based on the geometric principal axes of the talus of the subject. The major principal axis of the talus was defined the X-axis and the second principal axis was defined the Y-axis. The Z-axis was perpendicular to the XY-plane and coincided with the X- and Y-axis. The origin of the XYZ-coordinate system was located in the centroid of the talus. The positive X-axis was directed anteriorly, the positive Y-axis medially and the positive Z-axis proximally. The direction of the helical axis is represented by the normal vector  $n$ . Relative to the coordinate system the inclination angle of the helical axis is the angle between the XY-plane and the normal vector  $n$ . The deviation angle of the helical axis is the angle between the X-axis and the projection of the normal vector  $n$  on the XY-plane. Shown is the graphic representation of the XYZ-coordinate system with the normal vector  $n$  and talus of one subject.

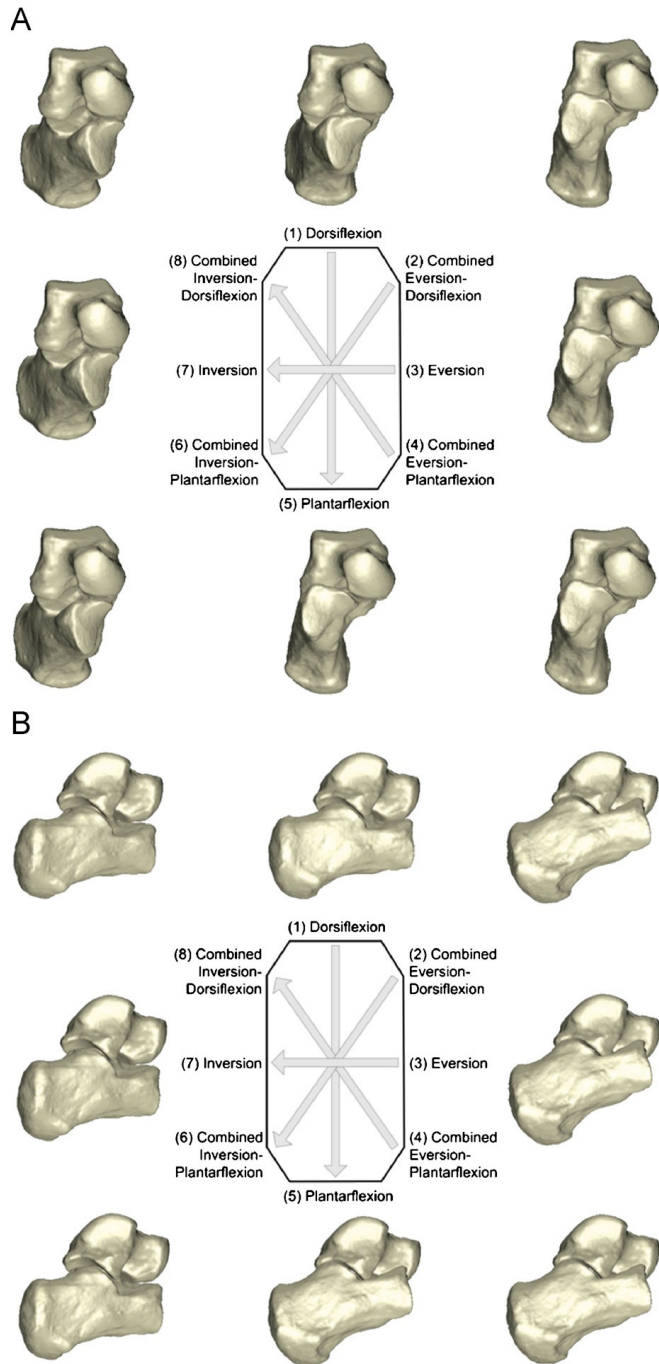


**Figure 3** Graphic representation of the position of the calcaneus relative to the talus for the eight extreme foot positions in one subject from an (A) anterior and (B) lateral view. The footplate is shown in the center as a reference to the extreme foot positions.

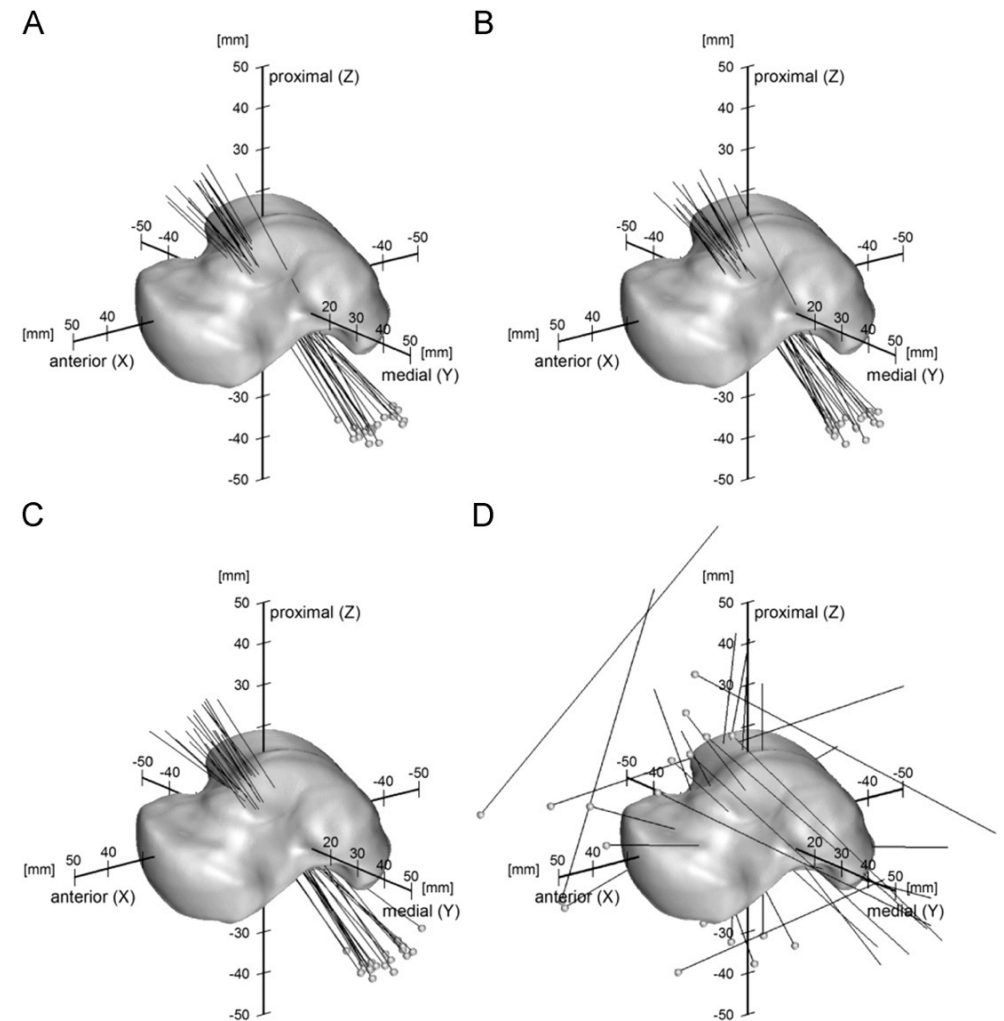


**Figure 4** Graphic representation of the helical axes for subtalar motion from (A) extreme eversion to extreme inversion, (B) extreme eversion-dorsiflexion to extreme inversion-plantarflexion, (C) extreme eversion-plantarflexion to extreme inversion-dorsiflexion, and (D) extreme dorsiflexion to extreme plantarflexion of twenty normal feet. The helical axes are grouped by overlying the talus-based XYZ-coordinate system of the subjects. The helical axes have a constant length of 100 mm. In all graphs the right talus of one subject is shown in the center of the XYZ-coordinate system from an anteromedial view.